JOURNAL OF SYNCHROTRON RADIATION

ISSN 1600-5775

Received 1 December 2017
Accepted 15 February 2018

Edited by Y. Amemiya, University of Tokyo, Japan

Keywords: X-ray beam-position monitor; diamond-fluorescence screen; feedback system.

X-ray beam-position feedback system with easy-to-use beam-position monitor

Jae Yeon Park,[a] Yesul Kim,[b] Sangsul Lee[a] and Jun Lim[a]*

[a]ITCC, Pohang Light Source, Jigokro 127, Pohang 37673, Republic of Korea, and [b]Soft Matter Physics Laboratory, School of Advanced Materials Science and Engineering, SKKU Advanced Institute of Nanotechnology (SAINT), Sungkyunkwan University, Suwon 16419, Republic of Korea. *Correspondence e-mail: limjun@postech.ac.kr

X-ray beam-position stability is indispensable in cutting-edge experiments using synchrotron radiation. Here, for the first time, a beam-position feedback system is presented that utilizes an easy-to-use X-ray beam-position monitor incorporating a diamond-fluorescence screen. The acceptable range of the monitor is above 500 µm and the feedback system maintains the beam position within 3 µm. In addition to being inexpensive, the system has two key advantages: it works without a scale factor for position calibration, and it has no dependence on X-ray energy, X-ray intensity, beam size or beam shape.

1. Introduction

Beam-position monitors have been in development since the 1950s when synchrotron light sources were first generated. The first monitors measured the beam diameters in metal foils such as carbon, aluminium and copper that produced photoelectrons in an ionization chamber (Blocker *et al.*, 1950). Beam position has been determined by measuring the electric current generated when an X-ray beam passes through a pair of metal blades or wires (Heald, 1986; Johnson & Oversluizen, 1989; Chen *et al.*, 1998; Xie *et al.*, 2001; Dhamgaye *et al.*, 2011). Inevitably, these intercept some part of the beam (Karlin *et al.*, 1992). To avoid interception, Bergonzo *et al.* (1999) measured photoelectrons generated by transmissive metallic crystals with quadrant electrodes. They used a lock-in amplifier to measure the beam position with a resolution of 2 µm.

Photodiodes have also been used to measure backscattered X-rays or fluorescent light (Alkire *et al.*, 2000; Kudo *et al.*, 2005; Tono *et al.*, 2011). Recently, quadrant electrodes using chemical vapor deposition (CVD) diamond have achieved response rates of ∼1 kHz and spatial resolution of <1 µm (Morse *et al.*, 2007; Desjardins *et al.*, 2014). In all of the above methods, the beam position is determined by a calculation associated with the difference-over-the-sum ($I_{\rm difference}/I_{\rm sum}$) equation (Schildkamp & Pradervand, 1995). Thus, a scale factor is required in order to convert the unit-less number ($I_{\rm difference}/I_{\rm sum}$) to distance. The beam position should also be calibrated by beam intensity, crystal thickness and X-ray energy (Bloomer *et al.*, 2016). The simplest means of beam-position monitoring is to capture the beam image that is projected onto a transparent screen using a camera. This method provides the shape, intensity and position of the beam simultaneously. Moreover, the screen is tilted to allow the beam to pass without blocking it (Fajardo & Ferrer, 1995), the detection range can be extended according to the screen size, and the instrumentation is simple. Indeed, the beam position is determined simply, according to the Gaussian fit of the beam

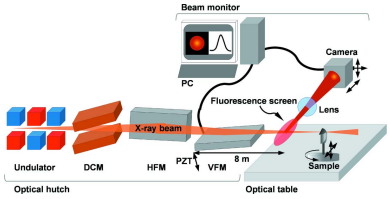

image. The initial beam-position monitor type used an X-ray camera to detect the Bragg reflection in a beryllium single crystal (Fajardo & Ferrer, 1995). Subsequently, helium gas, phosphorous and Kapton foil have also been used as screens (Koch & Riekel, 1996; Bunk *et al.*, 2005; Revesz & White, 2005; Fuchs *et al.*, 2007; Silfhout *et al.*, 2011). The recently developed CVD diamond for beam monitoring, with its excellent fluorescence-yield properties, facilitates a beam monitor-profile capture by employment of a CCD camera (Takahashi *et al.*, 2016).

In this paper, for the first time, we present a beam-position feedback system that utilizes an easy-to-use X-ray beam-position monitor incorporating a diamond-fluorescence screen. The beam monitor, which is installed in front of a sample stage, captures the fluorescence image on its screen, plots the beam profile, and determines the beam position. The beam position is utilized as feedback using a piezo-electric actuator for its control. We discuss the performance of the beam monitor and feedback system in the following sections.

2. Experiment method

The BL 7C spectroscopic X-ray nano-imaging (sXNI) beamline at Pohang Light Source-II is designed for spectral nano-resolution-imaging utilizing zone-plate-based transmission X-ray microscopy (TXM) (Lee *et al.*, 2017). Monochromatic X-rays are selected by a liquid-nitrogen-cooled double-crystal monochromator (DCM) and focused using a rhodium-coated horizontal focusing plane mirror (HFM) and a vertical focusing plane mirror (VFM). For microscopic imaging, normally, a tungsten objective zone plate of 40 nm outermost zone width, 150 µm diameter and 0.6 µm thickness is used. As a detector, a scintillator-coupled optical microscope (SOM) incorporating a thin scintillation crystal (15 µm-thick Tb:LSO), a 20× optical objective and a large-area CCD with 4096 × 4096 sensors of 9 µm pixel size is utilized. Typically, the lead time for computed tomography (CT) or spectral-mapped imaging of a sample is several minutes to a few hours. To maintain the beam position during this time is crucial, as it is well known that incident-beam instability causes contrast degradation and artifact formation in CT, and, moreover, incurs significant errors in spectral-mapped imaging. The beam monitor is installed between the VFM and the sample stage (Fig. 1). The fluorescence screen is a boron-doped CVD (B:CVD) diamond screen (30 µm thickness, 10 mm size, Diamond Materials GmbH). The diamond screen has a thermal conductivity of ∼2000 W mK^{-1} and a transmittance of ∼90% at 7 keV. Fluorescence images are collected using a CMOS camera (6.5 µm pixel size, 2048 × 2048 pixels) with a 10× objective. The beam profiles are fitted using a Gaussian function, based on which fitting, the center position is determined. In order to adjust the vertical beam position at the sample, a piezoelectric (PZT) actuator is installed at the front of the VFM, and a target position with a tolerance of 5 µm is set. Then, if the beam is out of position, the PZT actuator adjusts the pitch of the VFM in order to match the position of the beam to the set position.

3. Results

3.1. Beam position monitor

The center of the beam position is determined by the peak position of the beam profile. Fig. 2 shows an X-ray beam image and beam profiles. The focused X-ray beam size is 17 µm vertically and 296 µm horizontally. Considering the demagnification factors (3.9× vertically and 1.6× horizontally), the photon source size is quite similar to the previously measured value (Park *et al.*, 2014). Since TXM uses the central part of the focused beam, vertical beam movement has a more severe impact on CT and spectral-mapped imaging than horizontal movement. For that reason, we have installed a vertical feedback system. It should be noted that the beam profile is somewhat noisy, with many spikes, due primarily to the nature of the polycrystalline CVD diamond-fluorescence screen; this makes peak-position determination difficult. To explain, pure

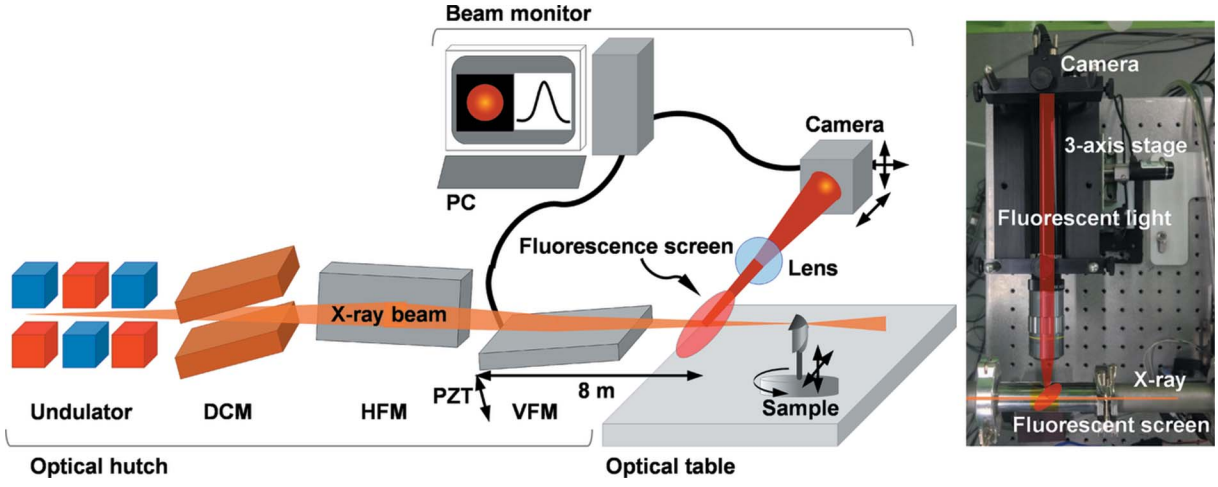

Figure 1
Beam-position monitoring and feedback system incorporating BL 7C sXNI beamline.

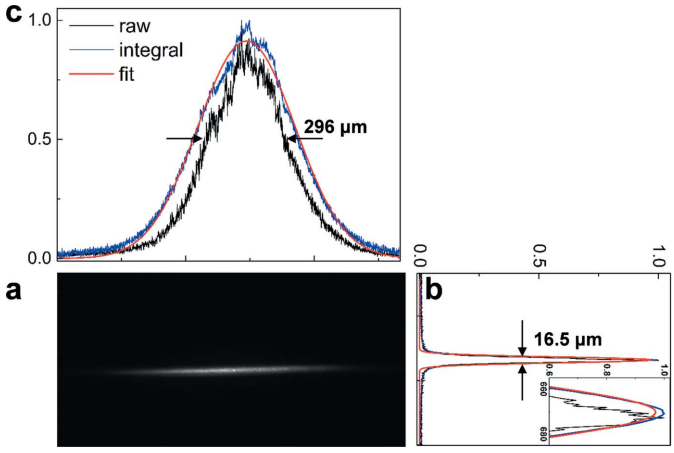

Figure 2
(*a*) Focused beam image; (*b*) vertical and (*c*) horizontal line profiles.

diamond never shows fluorescence with X-rays. Defects (*e.g.* vacancies and nitrogen) and impurities (*e.g.* boron) generate fluorescence in the visible regime when X-rays hit the screen; however, those are hardly uniformly distributed. Therefore, to increase the signal-to-noise ratio (SNR), we integrated the intensities of all of the rows and columns of the image, respectively. Then, we fitted the integrated signals using the Gaussian function, thereby determining the center position. The integral-Gaussian-fitting process worked within 50 ms, and so causes only a very limited delay. The whole machine control and data processing were written in *LabView*® software. Fig. 3 plots two-dimensional beam-position variation over 8 h at 1 Hz acquisition rate. Prior to the integration of the row and columns of the image, the raw data points are very irregularly spread, especially in the horizontal direction. However, after applying integral-Gaussian-fitting, the data points are merged within an area of 30 μm (V) × 25 μm (H). Fig. 4 plots the vertical beam position variation as a function of time. The red line is the median-filtered plot indicating the beam-position trend. This long-term drift can be related to external temperature changes of the experimental hall. Note that there is a periodic bump that repeats every 4.5 h. The inset shows a magnified view of the bump lasting for ∼15 minutes. The time of occurrence of the bump exactly matches the time to refill the liquid-nitrogen container in the cryo-cooler of the DCM. During refilling, the first crystal on

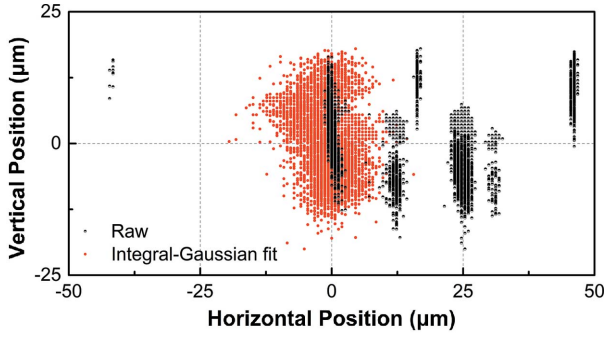

Figure 3
Two-dimensional beam-position variation over 8 h.

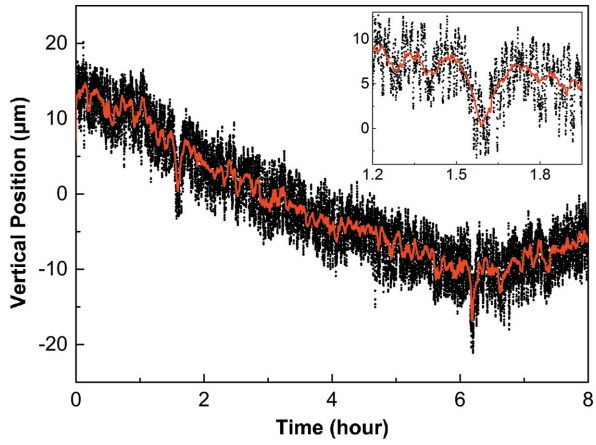

Figure 4
Vertical beam-position tracking on time axis. The beam shifted with long-term fluctuation over the course of hours (small vibrations over the course of minutes are represented in the inset).

the copper block connected to the cryo-cooler is moved by internal pressure changes. When the refilling is completed, the pressure settles down once again into the normal condition. The change in the beam position shown in Fig. 4 (inset) supports this explanation. Under these circumstances, a feedback system for stabilization of the beam position is necessary.

3.2. Beam feedback system

In order to stabilize the beam position at the sample, a PZT actuator is installed at the front of the VFM. The high-load PZT actuator (P-842.20, Physik Instruments) has a 30 μm travel range with a resolution of 0.3 nm. To verify the linear relationship between PZT motion and the beam position, we measured the beam position as a function of the PZT travel in 100 nm steps (Fig. 5). The figure shows that there is long-range (over 500 μm) linearity. When operating the actuator in 10 nm steps (inset), the beam position moves along the linear fitted line (red line) with a maximum error of 3 μm. Considering that the effective pixel resolution of the beam monitor is 0.65 μm,

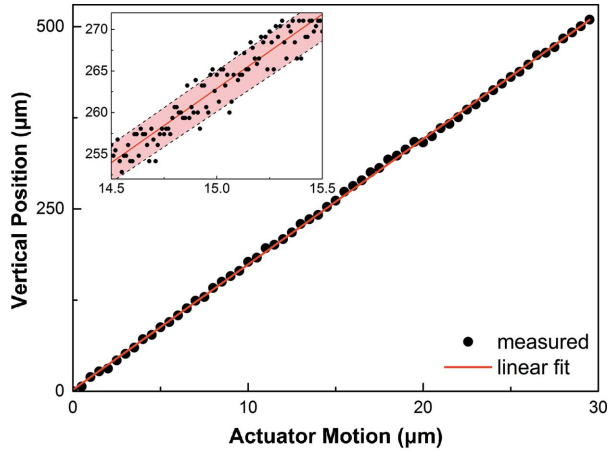

Figure 5
Beam-position response with piezoelectric actuator motion in VFM. The beam is shifted in direct proportion to the actuator motion.

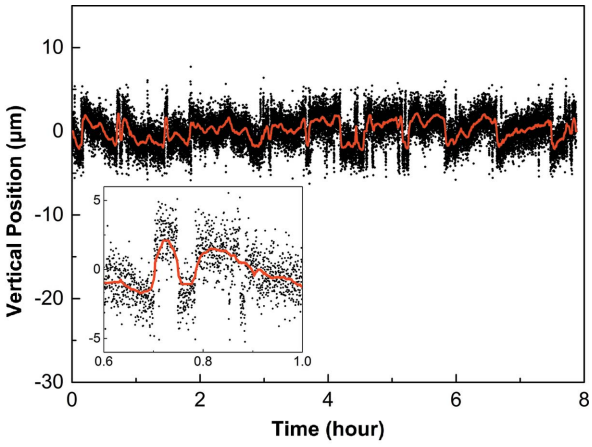

Figure 6
Beam-position tracking with feedback. The beam position was maintained for 8 h within ±5 μm displacement.

the position error seems somewhat large. There can be several reasons for this, one of which is the electrons' unstable motion at the source position. Recently, in an in-depth study of beam motion, we measured the beam position with a high-frame-rate camera of ∼5000 frames s^{-1}. The results will be presented in upcoming literature. The feedback system sets a target position with a tolerance of 5 μm. If the beam is out of position, the PZT actuator adjusts the pitch of the VFM in order to match the position of the beam to the set position. Fig. 6 shows 8 h of the beam-position tracking with the feedback system. The median-filtered plot clearly shows when the PZT actuator was operating (inset). The beam position was maintained at the target position within an error range of ±5 μm. For acquisition of reliable spectral-mapped imaging of chemical distributions using X-ray absorption near-edge structure (XANES) spectra, the beam position should be sufficiently stable during energy scanning of more than hundreds of electron volts. Fig. 7 shows one such example. We monitored the beam position changes within a 200 eV range in 20 eV intervals at the iron *K*-edge. The in-vacuum undulator was tapered to maintain a stable X-ray flux around the iron

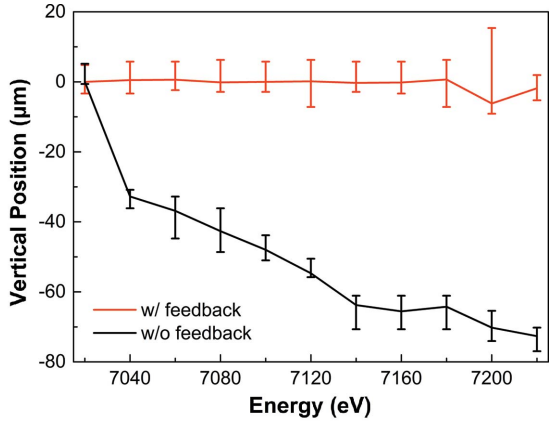

Figure 7
Beam-position tracking during DCM alignment with and without feedback.

K-edge. According to our recent report (Lee *et al.*, 2017), the pitch angle of the DCM varies gradually up to 60 μrad as the X-ray energy change is increased from 5 to 16 keV. The black line in the figure shows some of those changes. After applying feedback, the beam is stable at the target position within the error bar.

4. Conclusion

A beam-position feedback system has been developed that utilizes an easy-to-use X-ray beam-position monitor incorporating a diamond-fluorescence screen. To verify performance, the system was applied to the BL 7C sXNI beamline at Pohang Light Source-II. This simple beam-monitoring system can measure the beam position over 500 μm with a 3 μm uncertainty. Although not a high-end device (resolution, for example, is rather low), the system has practical advantages. This system can be usefully employed in general beamlines using X-rays of tens-of-micrometers size.

Funding information

This research was financially supported by the Basic Science Research Program through the National Research Foundation of Korea (NRF) funded by the Ministry of Science, ICT and Future Planning (2017R1A2B1002457; 2017R1C1B1011518).

References

Alkire, R. W., Rosenbaum, G. & Evans, G. (2000). *J. Synchrotron Rad.* **7**, 61–68.
Bergonzo, P., Brambilla, A., Tromson, D., Marshall, R. D., Jany, C., Foulon, F. & Goulon, J. (1999). *J.Synchrotron Rad.* **6**, 1–5.
Blocker, W., Kenney, R. W. & Panofsky, W. K. (1950). *Phys. Rev.* **79**, 419–428.
Bloomer, C., Rehm, G. & Dolbnya, I. P. (2016). *AIP Conf. Proc.* **1741**, 030022.
Bunk, O., Pfeiffer, F., Stampanoni, M., Patterson, B. D., Schulze-Briese, C. & David, C. (2005). *J. Synchrotron Rad.* **12**, 795–799.
Chen, J.-R., Ueng, T. S., Hsiung, G. Y., Lin, T. F., Lee, C. T., Tsai, S. L. & Chang, S.-L. (1998). *J. Synchrotron Rad.* **5**, 621–623.
Desjardins, K., Pomorski, M. & Morse, J. (2014). *J. Synchrotron Rad.* **21**, 1217–1223.
Dhamgaye, V. P., Lodha, G. S. & Kane, S. R. (2011). *Nucl. Instrum. Methods Phys. Res. A*, **659**, 525–527.
Fajardo, P. & Ferrer, S. (1995). *Rev. Sci. Instrum.* **66**, 1879–1881.
Fuchs, M. R., Holldack, K., Reichardt, G. & Mueller, U. (2007). *AIP Conf. Proc.* **879**, 1006–1009.
Heald, S. M. (1986). *Nucl. Instrum. Methods Phys. Res. A*, **246**, 411–412.
Johnson, E. D. & Oversluizen, T. (1989). *Rev. Sci. Instrum.* **60**, 1947–1950.
Karlin, B. A., Cowan, P. L. & Woicik, J. C. (1992). *Rev. Sci. Instrum.* **63**, 526–529.
Koch, A. & Riekel, C. (1996). *Rev. Sci. Instrum.* **67**, 1737–1740.
Kudo, T., Nishino, Y., Inoue, S. & Ishikawa, T. (2005). *J. Jpn. Soc. Synchrotron Radiat. Res.* **18**, 023108.
Lee, S., Kwon, I., Kim, J.-Y., Yang, S.-S., Kang, S. & Lim, J. (2017). *J. Synchrotron Rad.* **24**, 1276–1282.
Morse, J., Salomé, M., Berdermann, E., Pomorski, M., Cunningham, W. & Grant, J. (2007). *Diam. Relat. Mater.* **16**, 1049–1052.
Park, S. Y., Hong, C. K. & Lim, J. (2014). *Rev. Sci. Instrum.* **85**, 045116.

Revesz, P. & White, J. A. (2005). *Nucl. Instrum. Methods Phys. Res. A*, **540**, 470–479.
Schildkamp, W. & Pradervand, C. (1995). *Rev. Sci. Instrum.* **66**, 1956–1959.
Silfhout, R. van, Kachatkou, A., Kyele, N., Scott, P., Martin, T. & Nikitenko, S. (2011). *Opt. Lett.* **36**, 570–572.
Takahashi, S., Kudo, T., Sano, M., Watanabe, A. & Tajiri, H. (2016). *Rev. Sci. Instrum.* **87**, 083111.
Tono, K., Kudo, T., Yabashi, M., Tachibana, T., Feng, Y., Fritz, D. & Ishikawa, T. (2011). *Rev. Sci. Instrum.* **82**, 023108.
Xie, Y., Hu, T. D., Liu, T. & Xian, D. C. (2001). *Nucl. Instrum. Methods Phys. Res. A*, **467–468**, 256–259.